

Lattice dynamics in mono- and few-layer sheets of WS_2 and WSe_2

Weijie Zhao^{a,c,#}, Zohreh Ghorannevis^{a,c,#}, Amara Kiran Kumar^b, Jing Ren Pang^b, Minglin Toh^d, Xin Zhang^e, Christian Kloc^d, Ping Heng Tan^e, Goki Eda^{a,b,c,}*

^a Department of Physics, National University of Singapore, 2 Science Drive 3, Singapore 117542

^b Department of Chemistry, National University of Singapore, 3 Science Drive 3, Singapore 117543

^c Graphene Research Centre, National University of Singapore, 6 Science Drive 2, Singapore 117546

^d School of Materials Science and Engineering, Nanyang Technological University, N4.1 Nanyang Avenue, Singapore 639798

^e State Key Laboratory of Superlattices and Microstructures, Institute of Semiconductors, Chinese Academy of Sciences, Beijing 100083, China

* E-mail: g.eda@nus.edu.sg

Abstract

Thickness is one of the fundamental parameters that define the electronic, optical, and thermal properties of two-dimensional (2D) crystals. Phonons in molybdenum disulfide (MoS_2) were recently found to exhibit unique thickness dependence due to interplay between short and long range interactions. Here we report Raman spectra of atomically thin sheets of WS_2 and WSe_2 , isoelectronic compounds of MoS_2 , in the mono- to few-layer thickness regime. We show that, similar to the case of MoS_2 , the characteristic A_{1g}

and E_{2g}^1 modes exhibit stiffening and softening with increasing number of layers, respectively, with a small shift of less than 3 cm^{-1} due to large mass of the atoms. Thickness dependence is also observed in a series of multiphonon bands arising from overtone, combination, and zone edge phonons, whose intensity exhibit significant enhancement in excitonic resonance conditions. Some of these multiphonon peaks are found to be absent only in monolayers. These features provide a unique fingerprint and rapid identification for monolayer flakes.

Keywords: WS_2 , WSe_2 , monolayer, 2D crystals, Raman scattering

Introduction

Two-dimensional (2D) crystals derived from inorganic layered compounds offer a unique platform to explore fundamental condensed matter phenomena¹. Recently, tremendous interest has focused on 2D crystals of molybdenum disulfide (MoS₂) and other members of layered transition metal dichalcogenides (LTMDs) due to their intriguing electrical and optical properties²⁻¹³. A single monolayer of MoS₂ is a direct gap semiconductor with high in-plane carrier mobility and excellent gate coupling for electrostatic control of charge carrier density^{10, 11, 14}. Finite band gap and remarkable device performance make MoS₂ a complementary 2D material to graphene in nanoelectronics and photonics^{11, 15}. Further, sizable spin-orbit interaction along with broken inversion symmetry in monolayer MoS₂ allows optical access to valley degrees of freedom, demonstrating potential in novel spintronic and valleytronic devices^{4, 9, 16, 17}.

Tungsten-based LTMDs such as WS₂ and WSe₂ are isoelectronic to MoS₂ and exhibit a similar set of intriguing properties in 2D crystal form^{7, 11, 18-27}. Their monolayer consists of an X-M-X sandwich²⁸ (M and X denote transition metal and chalcogen atoms, respectively) with trigonal prismatic coordination as in MoS₂. Exfoliation of WS₂ and WSe₂ to mono- to few-layer thick sheets has been recently demonstrated by many groups^{7, 18, 19, 21, 25, 26, 29-33}. This has led to observation of remarkable field-modulated transport with large in-plane mobility^{11, 19}, indirect-to-direct band gap transition upon isolation of single layers^{7, 21, 22, 32}, robust valley polarization²⁵, second harmonic generation⁷, and tightly bound trions²⁵. Spin-orbit interaction in these materials is substantially larger³⁴⁻³⁹ compared to that in MoS₂ thus offering a robust platform to study spin and valley physics.

While confinement effects on the electronic and excitonic dispersion relation in atomically thin sheets of tungsten dichalcogenides has been extensively studied to date^{21, 34, 39-41}. On the other hand, little has been understood about the phonon behaviors

in these 2D crystals. Lee et al.⁴² recently reported that phonon frequency of atomically thin MoS₂ flakes exhibits unique thickness dependence where two characteristic Raman active modes A_{1g} and E_{2g}^1 exhibit opposite trends with thickness. Specifically, the A_{1g} mode, which involves the out-of-plane displacement of S atoms, is found to stiffen with increasing number of layers. In contrast, the E_{2g}^1 mode, which involves the in-plane displacement of Mo and S atoms, exhibits softening with flake thickness. Further studies⁴³ have shown that the shift in the A_{1g} mode can be explained by the interlayer interaction of S atoms in the neighboring planes, while the unexpected trend of the E_{2g}^1 mode is explained by dielectric screening of long range Coulomb interaction.

Although these phonon modes in tungsten dichalcogenides were expected to follow the same trends as in MoS₂^{42, 44, 45}, there have been conflicting reports on the thickness dependence of phonon modes in WS₂ and WSe₂ sheets in mono- to few-layer regime.^{7, 22, 26, 31, 32, 46, 47} For WSe₂, this is partly attributed to the lack of consensus on the assignment of A_{1g} mode^{7, 31, 47}. Of particular interest is the discrepancy between the experimental with the theoretical results where latter suggest that A_{1g} and E_{2g}^1 are degenerate in WSe₂.⁴⁷ Further, behavior of multiphonon modes which contain rich information on the electronic and phonon dispersion relation⁴⁶ are largely unexplored. A detailed study of the phonon properties needs to be conducted in order to achieve valuable insight into phonon confinement effects in these intriguing 2D materials.

Here, we report detailed studies on the Raman spectra of mechanically exfoliated mono- and few-layer WS₂ and WSe₂ flakes. With the use of polarized spectroscopy, we demonstrate that for both materials the A_{1g} and E_{2g}^1 modes exhibit opposite shift with increasing number of layers indicating the effects of both short and long range

interactions. We find that these phonon modes are degenerate in monolayer WSe_2 as predicted by theory⁴⁷ but the degeneracy is lifted in multilayers. We further discuss excitonic resonance Raman spectra for WS_2 and WSe_2 where a series of multiphonon bands are observed. We demonstrate that some of these features contain unique fingerprints of monolayer flakes.

Results and Discussion

Figure 1a shows the optical contrast or differential reflectance spectra of 3L WS_2 and WSe_2 flakes. The optical contrast is defined as $(R_{S+Q} - R_Q)/R_Q$ where R_{S+Q} and R_Q are the reflected light intensities from the quartz substrate with and without samples, respectively^{2, 48}. This quantity is proportional to absorbance for ultrathin samples and its spectral response can be interpreted as absorption spectrum^{2, 21, 48}. Characteristic excitonic absorption peaks A and B are observed along with a higher energy density of states peak C and split exciton peaks A' and B'. The A and B excitonic absorption peaks arise from optical transitions involving spin-orbit split valence band and degenerate conduction band at the K point of the Brillouin zone^{34, 49}. In this study, we investigate Raman scattering with three excitation wavelengths (472, 532, and 633 nm). The 532 nm excitation is in resonance with the B exciton peak of WS_2 and A' exciton peak of WSe_2 . On the other hand, 473 nm excitation is roughly in resonance with the interband transition peak C for WS_2 and interband absorption continuum for WSe_2 . The 633 nm excitation is in resonance with the A excitonic absorption for WS_2 and interband absorption but close to the B excitonic absorption for WSe_2 . Raman features of both WS_2 and WSe_2 strongly depend on the excitation conditions due to energy dependent Raman cross section of the phonons (See Supporting Information for details). The

absorption peaks shift slightly with flake thickness²¹ but the resonance conditions remain largely unaltered.

The crystal structure of 2H-WX₂ belongs to D_{6h}^4 point group. There are 18 lattice dynamical modes at the center of the Brillouin zone (Γ point)⁵⁰⁻⁵⁴. The irreducible representations of zone center phonons are as follows^{50, 51, 54}:

$$\Gamma = A_{1g} + 2A_{2u} + B_{1u} + 2B_{2g} + E_{1g} + 2E_{1u} + E_{2u} + 2E_{2g}$$

The atomic displacement of the four Raman active modes A_{1g} , E_{1g} , E_{2g}^1 and E_{2g}^2 is shown in Figure 1b. The A_{1g} mode is an out-of-plane vibration involving only the chalcogen atoms while the E_{2g}^1 mode involves in-plane displacement of transition metal and chalcogen atoms^{50, 51}. The E_{2g}^2 mode is shear mode corresponding to the vibration of two rigid layers against each other and appears at very low frequencies ($< 50 \text{ cm}^{-1}$)^{26, 45, 50, 51, 53, 55-58}. The E_{1g} mode, which is an in-plane vibration of only the chalcogen atoms, is forbidden in the back-scattering Raman configuration^{50, 51}.

Monolayer WX₂ belongs to D_{3h} point group and has 9 modes at the Brillouin zone center.⁴³ The rigid layer shear mode E_{2g}^2 is absent in monolayers^{26, 45, 55, 58}. Unpolarized Raman spectrum of bulk WS₂ obtained with 473 nm excitation shows characteristic A_{1g} and E_{2g}^1 peaks that are clearly separated and of similar intensity (Figure 1c). In contrast, only one prominent peak can be clearly seen in bulk WSe₂ spectrum in the frequency region where we expect A_{1g} and E_{2g}^1 peaks⁵⁷ (See Supporting Information). In 633 nm excitation condition, however, multiple peaks are evident in this region (Figure 1d). There have been inconsistent reports on the assignment of these peaks^{7, 31, 32, 47}. We

demonstrate below that two peaks found at 248 and 250 cm^{-1} are E_{2g}^1 and A_{1g} peaks in agreement with the previous study by Mead and Irwin⁵⁷.

In polarized back-scattering Raman spectroscopy, A_{1g} mode is allowed in parallel polarization ($Z(XX)\bar{Z}$) but forbidden in cross polarization ($Z(XY)\bar{Z}$) conditions⁴⁵. Thus A_{1g} mode can be identified by observing Raman spectra in the two polarization conditions. Figure 2a shows the parallel and cross polarized Raman spectra of 1 to 5L and bulk WS_2 flakes obtained with 473 nm excitation. The disappearance of the peak at $\sim 420 \text{ cm}^{-1}$ in cross polarization confirms that it is a A_{1g} mode. The peak at around $\sim 356 \text{ cm}^{-1}$ with no polarization dependence is a E_{2g}^1 mode. The peak positions agree well with the previous reports^{53, 54}. As shown in Figure 2, the A_{1g} phonon stiffens and E_{2g}^1 phonon softens with increasing flake thickness similar to the case of MoS_2 ⁴² and as predicted by recent theoretical studies⁴³. The difference in the frequency of these peaks is 60 and 65 cm^{-1} for monolayer and bulk samples, respectively (Figure 2b). The intensity ratios (A_{1g} / E_{2g}^1) show a similar trend as seen in MoS_2 . The FWHM is found to consistently decrease with increasing number of layers (Figure 2c).

Raman spectra of WSe_2 flakes measured in two polarization configurations and with 633 nm excitation are shown in Figure 3a. In contrast to the case in WS_2 , the parallel polarization spectra of WSe_2 flakes exhibit one prominent peak with a small shoulder in the frequency region where A_{1g} and E_{2g}^1 peaks are expected to be observed⁵⁷. The main peak upshifts from 249.5 to 251 cm^{-1} with increasing flake thickness from monolayer to bulk. In cross polarized spectra, a single peak is observed in this frequency region. This peak is found to downshift with increasing flake thickness. The peak intensity is normalized in Figure 3a to show this trend. The opposite thickness

dependence and polarization dependence indicates that they are indeed A_{1g} and E_{2g}^1 modes. The peak at 257 cm^{-1} did not show consistent polarization dependence, as shown in the Figure S2 of the Supporting Information. This peak was reported to be the A_{1g} phonon by some groups^{7, 31, 47}. As shown in Figure 1 and Figure S2, this peak is very broad, which is uncharacteristic for a first order Raman peak, and shows only weak dependence on the polarization configuration. It is assigned to the 2LA(M) phonon here according to the theoretical calculation⁵⁹. Similar to MoS_2 and WS_2 , the A_{1g} (E_{2g}^1) phonon of WSe_2 stiffens (softens) with increase in flake thickness (Figure 3b). The key difference is that the two modes become virtually degenerate in the single layer limit. We note that in 473 nm excitation condition, only a single peak appears in the unpolarized and parallel polarized spectra due to relatively weak E_{2g}^1 peak. Similar to MoS_2 and WS_2 , the general trends in FWHM and intensity ratio of A_{1g} and E_{2g}^1 peaks were consistent with those of MoS_2 and WS_2 (Figure 3c).

Figure 4 shows the comparison of frequencies and shifts for A_{1g} and E_{2g}^1 peaks in different Group 6 TMDs. The E_{2g}^1 frequency consistently decreases with increasing “molecular weight” of the unit cell. On the other hand, a distinct jump is found in the A_{1g} frequency between the MS_2 and MSe_2 groups. This reflects the difference in the chalcogen atomic masses. Difference in phonon frequencies between monolayer and bulk flakes (ΔA_{1g} and ΔE_{2g}^1) is also highly dependent on the material (Figure 4b). Stiffening and softening of the modes are most prominently observed in MoS_2 where A_{1g} and E_{2g}^1 peaks shift by 4 and 2 cm^{-1} , respectively.⁴² The shift becomes less pronounced with “heavier” MX_2 with one exception of E_{2g}^1 mode of MoSe_2 which has

been reported to exhibit comparatively large shift ($\sim 3.6 \text{ cm}^{-1}$)¹⁸. Due to the heavy atoms, WSe₂ shows the smallest thickness dependent shift ($\sim 1.3 \text{ cm}^{-1}$) for the two modes.

The small thickness dependence of the A_{1g} and E_{2g}^1 peaks in WS₂ and WSe₂ imply that they are not ideal fingerprints for identifying the number of layers. In the following, we discuss thickness dependence of other phonons that are observed in excitonic resonance conditions. We focus the following discussions on 532 nm resonance. Details of results obtained with 633 nm excitation are presented in the Supporting Information.

Figures 5 and 6 show unpolarized Raman spectra obtained with 532 nm excitation, which is in resonance with B and A' exciton absorption peaks for WS₂ and WSe₂, respectively. A series of overtone and combination peaks arising from the Brillouin zone center and zone edge phonons are observed along with the first order E_{2g}^1 and A_{1g} modes. Detailed assignments of multiphonon bands according to recently calculated phonon dispersion curves^{43, 59} are summarized in Table S1 of the Supporting Information.

The most prominent resonance feature emerges near the E_{2g}^1 peak for both WS₂ and WSe₂. This peak, labeled as 2LA(M), is a second-order Raman mode due to LA phonons at the M point in the Brillouin zone^{43, 54}. We found that the 2LA(M) mode shows distinct downshift of 5 cm^{-1} with increasing flake thickness from monolayer to trilayer for WSe₂ (See Supporting Information for details). In contrast, the same mode in WS₂ showed no obvious trend. The first-order phonon LA(M) in both WS₂ and WSe₂ is widely involved in the overtone and combination mode of other zone edge phonons, similar to the case of MoS₂^{44, 60}.

We observed similar multiphonon bands and 2LA(M) features with 633 nm excitation, which is in resonance with A and B exciton absorption for WS₂ and WSe₂, respectively (See Supporting Information for details). These results indicate that the enhancement of the total Raman cross section at excitonic resonance in which excitons serve as the

intermediate state is stronger compared to that of interband resonance. The strong enhancement at excitonic resonance is attributed to the characteristics of excitons in layered materials such as large binding energy, enhanced oscillator strength, and small damping constant^{28, 34, 61-63}. It should be noted that resonance Raman features are also seen with 473 nm excitation but to a lesser degree (See Supporting Information for details).

Figure 5b highlights that a peak at $\sim 310 \text{ cm}^{-1}$, which is consistently observed for multilayer flakes of WS_2 , is absent in monolayers. The origin of this mode is not clear, however, its absence in monolayers suggests that it may be related to rigid layer shear. Relatively large frequency of this peak suggests that it is a combination of low-frequency modes^{26, 45} with another phonon mode. Figure 6b shows that similar behavior is observed in a peak located around 308 cm^{-1} for WSe_2 . This peak is absent in monolayers and shows clear softening with increasing thickness. Thus, it is possibly a combination mode of a shear and E_{2g}^1 modes. Further evidence is required to verify our speculations on the origin of the peak. These features are useful for quickly identifying WS_2 and WSe_2 monolayers.

Conclusions

In summary, we study Raman scattering in mono- and few-layer WS_2 and WSe_2 flakes. Characteristic A_{1g} and E_{2g}^1 phonon modes show distinct thickness dependence where the former stiffens and the latter softens with increasing number of layers. While the general behaviors are similar to the case of MoS_2 , the thickness dependent shift of A_{1g} and E_{2g}^1 peaks is considerably smaller for WS_2 and WSe_2 possibly due to the

larger atomic masses. The A_{1g} and E_{2g}^1 modes in WSe_2 exhibit small frequency difference in multilayers and become degenerate in single layers. Presence of E_{2g}^1 peak can be verified in cross polarized spectra where the A_{1g} mode is forbidden. Excitonic resonance Raman scattering reveals a series of multiphonon bands involving the Raman inactive phonons at Brillouin zone center and zone edge phonons. We demonstrate that some of the multiphonon bands are absent in monolayers but activated in multilayers, suggesting possible contributions from the low frequency modes. These features allow rapid and unambiguous identification of monolayers.

Methods

Bulk crystals of 2H- WS_2 and 2H- WSe_2 were grown by chemical vapor transport (CVT). Bulk crystals of 2H- WS_2 and 2H- WSe_2 crystals were mechanically exfoliated on to quartz substrates and used for subsequent spectroscopic characterization. The number of layers in the flakes was confirmed by optical contrast and atomic force microscope (AFM)²¹. The optical contrast was measured using a tungsten-halogen lamp coupled to a Raman spectrometer. Raman spectra were acquired in ambient conditions using 473, 532 and 633 nm laser excitations. The laser power on the sample during Raman measurement was kept below 150 μ W in order to avoid sample damage and excessive heating. A 2400 grooves/mm grating was used to achieve spectral resolution of below 1 cm^{-1} . The silicon Raman mode at 520 cm^{-1} was used for the calibration prior to measurements.

Acknowledgment

G Eda acknowledges Singapore National Research Foundation for funding the research under NRF Research Fellowship (NRF-NRFF2011-02). PH Tan thanks the supports from NSFC under grants 10934007 and 11225421.

Supporting Information

Detailed Raman spectra obtained with three laser excitations and possible assignments of the multiphonon bands are presented in the Supporting Information.

References

1. Novoselov, K. S.; Jiang, D.; Schedin, F.; Booth, T. J.; Khotkevich, V. V.; Morozov, S. V.; Geim, A. K., Two-dimensional atomic crystals. *Proceedings of the National Academy of Sciences of the United States of America* **2005**, *102* (30), 10451-10453.
2. Mak, K. F.; Lee, C.; Hone, J.; Shan, J.; Heinz, T. F., Atomically Thin MoS₂: A New Direct-Gap Semiconductor. *Physical Review Letters* **2010**, *105* (13), 136805.
3. Coleman, J. N.; Lotya, M.; O'Neill, A.; Bergin, S. D.; King, P. J.; Khan, U.; Young, K.; Gaucher, A.; De, S.; Smith, R. J.; Shvets, I. V.; Arora, S. K.; Stanton, G.; Kim, H.-Y.; Lee, K.; Kim, G. T.; Duesberg, G. S.; Hallam, T.; Boland, J. J.; Wang, J. J.; Donegan, J. F.; Grunlan, J. C.; Moriarty, G.; Shmeliov, A.; Nicholls, R. J.; Perkins, J. M.; Grievson, E. M.; Theuwissen, K.; McComb, D. W.; Nellist, P. D.; Nicolosi, V., Two-Dimensional Nanosheets Produced by Liquid Exfoliation of Layered Materials. *Science* **2011**, *331* (6017), 568-571.
4. Mak, K. F.; He, K. L.; Shan, J.; Heinz, T. F., Control of valley polarization in monolayer MoS₂ by optical helicity. *Nat Nanotechnol* **2012**, *7* (8), 494-498.
5. Splendiani, A.; Sun, L.; Zhang, Y.; Li, T.; Kim, J.; Chim, C.-Y.; Galli, G.; Wang, F., Emerging Photoluminescence in Monolayer MoS₂. *Nano Letters* **2010**, *10* (4), 1271-1275.

6. Ross, J. S.; Wu, S.; Yu, H.; Ghimire, N. J.; Jones, A. M.; Aivazian, G.; Yan, J.; Mandrus, D. G.; Xiao, D.; Yao, W.; Xu, X., Electrical control of neutral and charged excitons in a monolayer semiconductor. *Nature Communications* **2013**, *4*, 1474.
7. Zeng, H.; Liu, G. B.; Dai, J.; Yan, Y.; Zhu, B.; He, R.; Xie, L.; Xu, S.; Chen, X.; Yao, W.; Cui, X., Optical signature of symmetry variations and spin-valley coupling in atomically thin tungsten dichalcogenides. *SCIENTIFIC REPORTS* **2012**, doi:10.1038/srep01608.
8. Yin, Z.; Li, H.; Li, H.; Jiang, L.; Shi, Y.; Sun, Y.; Lu, G.; Zhang, Q.; Chen, X.; Zhang, H., Single-Layer MoS₂ Phototransistors. *ACS Nano* **2011**, *6* (1), 74-80.
9. Cao, T.; Wang, G.; Han, W. P.; Ye, H. Q.; Zhu, C. R.; Shi, J. R.; Niu, Q.; Tan, P. H.; Wang, E.; Liu, B. L.; Feng, J., Valley-selective circular dichroism of monolayer molybdenum disulphide. *Nature Communications* **2012**, *3*.
10. Radisavljevic, B.; Radenovic, A.; Brivio, J.; Giacometti, V.; Kis, A., Single-layer MoS₂ transistors. *Nat Nanotechnol* **2011**, *6* (3), 147-150.
11. Wang, Q. H.; Kalantar-Zadeh, K.; Kis, A.; Coleman, J. N.; Strano, M. S., Electronics and optoelectronics of two-dimensional transition metal dichalcogenides. *Nat Nanotechnol* **2012**, *7* (11), 699-712.
12. Mak, K. F.; He, K.; Lee, C.; Lee, G. H.; Hone, J.; Heinz, T. F.; Shan, J., Tightly bound trions in monolayer MoS₂. *Nature Materials* **2013**, *12*, 207.
13. Feng, J.; Qian, X.; Huang, C.-W.; Li, J., Strain-engineered artificial atom as a broad-spectrum solar energy funnel. *Nature Photonics* **2012**, *6*, 866-872.
14. Pu, J.; Yomogida, Y.; Liu, K.-K.; Li, L.-J.; Iwasa, Y.; Takenobu, T., Highly Flexible MoS₂ Thin-Film Transistors with Ion Gel Dielectrics. *Nano Letters* **2012**, *12* (8), 4013-4017.
15. Song, X.; Hu, J.; Zeng, H., Two-dimensional semiconductors: recent progress and future perspectives. *Journal of Materials Chemistry C* **2013**, *1* (17), 2952-2969.
16. Zeng, H. L.; Dai, J. F.; Yao, W.; Xiao, D.; Cui, X. D., Valley polarization in MoS₂ monolayers by optical pumping. *Nat Nanotechnol* **2012**, *7* (8), 490-493.
17. Sallen, G.; Bouet, L.; Marie, X.; Wang, G.; Zhu, C. R.; Han, W. P.; Lu, Y.; Tan, P. H.; Amand, T.; Liu, B. L.; Urbaszek, B., Robust optical emission polarization in MoS₂ monolayers through selective valley excitation. *Physical Review B* **2012**, *86* (8), 081301.
18. Tongay, S.; Zhou, J.; Ataca, C.; Lo, K.; Matthews, T. S.; Li, J.; Grossman, J. C.; Wu, J., Thermally Driven Crossover from Indirect toward Direct Bandgap in 2D Semiconductors: MoSe₂ versus MoS₂. *Nano Letters* **2012**.
19. Fang, H.; Chuang, S.; Chang, T. C.; Takei, K.; Takahashi, T.; Javey, A., High-Performance Single Layered WSe₂ p-FETs with Chemically Doped Contacts. *Nano Letters* **2012**, *12* (7), 3788-3792.
20. Benameur, M. M.; Radisavljevic, B.; Heron, J. S.; Sahoo, S.; Berger, H.; Kis, A., Visibility of dichalcogenide nanolayers. *Nanotechnology* **2011**, *22* (12).
21. Zhao, W.; Ghorannevis, Z.; Chu, L.; Toh, M.; Kloc, C.; Tan, P.-H.; Eda, G., Evolution of electronic structure in atomically thin sheets of WS₂ and WSe₂. *ACS Nano* **2013**, *7*, 791.
22. Gutiérrez, H. R.; Perea-López, N.; Elías, A. L.; Berkdemir, A.; Wang, B.; Lv, R.; López-Urías, F.; Crespi, V. H.; Terrones, H.; Terrones, M., Extraordinary room-temperature photoluminescence in WS₂ monolayers. *Nano Letters* **2012**, DOI: 10.1021/nl3026357.

23. Late, D. J.; Liu, B.; Matte, H. S. S. R.; Rao, C. N. R.; Dravid, V. P., Rapid Characterization of Ultrathin Layers of Chalcogenides on SiO₂/Si Substrates. *Advanced Functional Materials* **2012**, *22* (9), 1894-1905.
24. Matte, H. S. S. R.; Plowman, B.; Datta, R.; Rao, C. N. R., Graphene analogues of layered metal selenides. *Dalton Transactions* **2011**, *40* (40), 10322-10325.
25. Jones, A. M.; Hongyi, Y.; Ghimire, N.; Wu, S.; Aivazian, G.; Ross, J. S.; Zhao, B.; Yan, J.; Mandrus, D.; Xiao, D.; Yao, W.; Xu, X., Optical Generation of Excitonic Valley Coherence in Monolayer WSe₂. *arXiv:1303.5318* **2013**.
26. Zhao, Y.; Luo, X.; Li, H.; Zhang, J.; Araujo, P. T.; Gan, C. K.; Wu, J.; Zhang, H.; Quek, S. Y.; Dresselhaus, M. S.; Xiong, Q., Interlayer Breathing and Shear Modes in Few-Trilayer MoS₂ and WSe₂. *Nano Letters* **2013**, *13* (3), 1007-1015.
27. Horzum, S.; Sahin, H.; Cahangirov, S.; Cudazzo, P.; Rubio, A.; Serin, T.; Peeters, F. M., Phonon softening and direct to indirect band gap crossover in strained single-layer MoSe₂. *Physical Review B* **2013**, *87* (12), 125415.
28. Wilson, J. A.; Yoffe, A. D., Transition Metal Dichalcogenides Discussion and Interpretation of Observed Optical, Electrical and Structural Properties. *Advances in Physics* **1969**, *18* (73), 193-&.
29. Eda, G.; Fujita, T.; Yamaguchi, H.; Voiry, D.; Chen, M.; Chhowalla, M., Coherent Atomic and Electronic Heterostructures of Single-Layer MoS₂. *ACS Nano* **2012**, *6* (8), 7311-7317.
30. Eda, G.; Yamaguchi, H.; Voiry, D.; Fujita, T.; Chen, M.; Chhowalla, M., Photoluminescence from Chemically Exfoliated MoS₂. *Nano Letters* **2011**, *11* (12), 5111-5116.
31. Li, H.; Lu, G.; Wang, Y.; Yin, Z.; Cong, C.; He, Q.; Wang, L.; Ding, F.; Yu, T.; Zhang, H., Mechanical Exfoliation and Characterization of Single- and Few-Layer Nanosheets of WSe₂, TaS₂, and TaSe₂. *Small* **2012**, *doi: 10.1002/sml.201202919*.
32. Tonndorf, P.; Schmidt, R.; Böttger, P.; Zhang, X.; Börner, J.; Liebig, A.; Albrecht, M.; Kloc, C.; Gordan, O.; Zahn, D. R. T.; Vasconcellos, S. M. d.; Bratschitsch, R., Photoluminescence emission and Raman response of monolayer MoS₂, MoSe₂, and WSe₂. *Optics Express* **2013**, *21*, 4908.
33. Zeng, Z. Y.; Yin, Z. Y.; Huang, X.; Li, H.; He, Q. Y.; Lu, G.; Boey, F.; Zhang, H., Single-Layer Semiconducting Nanosheets: High-Yield Preparation and Device Fabrication. *Angew Chem Int Edit* **2011**, *50* (47), 11093-11097.
34. Coehoorn, R.; Haas, C.; de Groot, R. A., Electronic structure of MoSe₂, MoS₂, and WSe₂. II. The nature of the optical band gaps. *Physical Review B* **1987**, *35* (12), 6203-6206.
35. Ding, Y.; Wang, Y.; Ni, J.; Shi, L.; Shi, S.; Tang, W., First principles study of structural, vibrational and electronic properties of graphene-like MX₂ (M=Mo, Nb, W, Ta; X=S, Se, Te) monolayers. *Physica B: Condensed Matter* **2011**, *406* (11), 2254-2260.
36. Cheiwchanamngij, T.; Lambrecht, W. R. L., Quasiparticle band structure calculation of monolayer, bilayer, and bulk MoS₂. *Physical Review B* **2012**, *85* (20), 205302.
37. Ramasubramaniam, A., Large excitonic effects in monolayers of molybdenum and tungsten dichalcogenides. *Physical Review B* **2012**, *86* (11), 115409.

38. Yun, W. S.; Han, S. W.; Hong, S. C.; Kim, I. G.; Lee, J. D., Thickness and strain effects on electronic structures of transition metal dichalcogenides: 2H-MX₂ semiconductors (M = Mo, W; X = S, Se, Te). *Physical Review B* **2012**, *85* (3), 033305.
39. Zhu, Z. Y.; Cheng, Y. C.; Schwingenschlögl, U., Giant spin-orbit-induced spin splitting in two-dimensional transition-metal dichalcogenide semiconductors. *Physical Review B* **2011**, *84* (15), 153402.
40. Consadori, F.; Frindt, R. F., Crystal Size Effects on the Exciton Absorption Spectrum of WSe₂. *Physical Review B* **1970**, *2* (12), 4893-4896.
41. Frindt, R. F., Optical Absorption of a Few Unit-Cell Layers of MoS₂. *Physical Review* **1965**, *140* (2A), A536-A539.
42. Lee, C.; Yan, H.; Brus, L. E.; Heinz, T. F.; Hone, J.; Ryu, S., Anomalous Lattice Vibrations of Single- and Few-Layer MoS₂. *ACS Nano* **2010**, *4* (5), 2695-2700.
43. Molina-Sanchez, A.; Wirtz, L., Phonons in single-layer and few-layer MoS₂ and WS₂. *Physical Review B* **2011**, *84* (15).
44. Chakraborty, B.; Matte, H. S. S. R.; Sood, A. K.; Rao, C. N. R., Layer-dependent resonant Raman scattering of a few layer MoS₂. *Journal of Raman Spectroscopy* **2012**, DOI: 10.1002/jrs.4147.
45. Zhang, X.; Han, W. P.; Wu, J. B.; Milana, S.; Lu, Y.; Li, Q. Q.; Ferrari, A. C.; Tan, P. H., Raman spectroscopy of shear and layer breathing modes in multilayer MoS₂. *Physical Review B* **2012**, *87*, 115413.
46. Berkdemir, A.; Gutierrez, H. R.; Botello-Mendez, A. R.; Perea-Lopez, N.; Elias, A. L.; Chia, C.-I.; Wang, B.; Crespi, V. H.; Lopez-Urias, F.; Charlier, J.-C.; Terrones, H.; Terrones, M., Identification of individual and few layers of WS₂ using Raman Spectroscopy *SCIENTIFIC REPORTS* **2013**, doi:10.1038/srep01755.
47. Sahin, H.; Tongay, S.; Horzum, S.; Fan, W.; Zhou, J.; Li, J.; Wu, J.; Peeters, F. M., Anomalous Raman spectra and thickness-dependent electronic properties of WSe₂. *Physical Review B* **2013**, *87* (16), 165409.
48. Mak, K. F.; Sfeir, M. Y.; Wu, Y.; Lui, C. H.; Misewich, J. A.; Heinz, T. F., Measurement of the Optical Conductivity of Graphene. *Physical Review Letters* **2008**, *101* (19), 196405.
49. Beal, A. R.; Liang, W. Y.; Knights, J. C., Transmission Spectra of Some Transition-Metal Dichalcogenides .2. Group Via - Trigonal Prismatic Coordination. *J Phys Part C Solid* **1972**, *5* (24), 3540-&.
50. Verble, J. L.; Wieting, T. J., Lattice Mode Degeneracy in MoS₂ and Other Layer Compounds. *Physical Review Letters* **1970**, *25* (6), 362-365.
51. Wieting, T. J.; Verble, J. L., Infrared and Raman Studies of Long-Wavelength Optical Phonons in Hexagonal MoS₂. *Physical Review B* **1971**, *3* (12), 4286-4292.
52. Sekine, T.; Izumi, M.; Nakashizu, T.; Uchinokura, K.; Matsuura, E., Raman-Scattering and Infrared Reflectance in 2h-Mose₂. *J Phys Soc Jpn* **1980**, *49* (3), 1069-1077.
53. Sekine, T.; Nakashizu, T.; Toyoda, K.; Uchinokura, K.; Matsuura, E., Raman scattering in layered compound 2H-WS₂. *Solid State Communications* **1980**, *35* (4), 371-373.
54. Sourisseau, C.; Cruège, F.; Fouassier, M.; Alba, M., Second-order Raman effects, inelastic neutron scattering and lattice dynamics in 2H-WS₂. *Chem Phys* **1991**, *150* (2), 281-293.

55. Plechinger, G.; Heydrich, S.; Eroms, J.; Weiss, D.; Schuller, C.; Korn, T., Raman spectroscopy of the interlayer shear mode in few-layer MoS₂ flakes. *Applied Physics Letters* **2012**, *101* (10), 101906-3.
56. Tan, P. H.; Han, W. P.; Zhao, W. J.; Wu, Z. H.; Chang, K.; Wang, H.; Wang, Y. F.; Bonini, N.; Marzari, N.; Pugno, N.; Savini, G.; Lombardo, A.; Ferrari, A. C., The shear mode of multilayer graphene. *Nature Materials* **2012**, *11* (4), 294-300.
57. Mead, D. G.; Irwin, J. C., Long wavelength optic phonons in WSe₂. *Canadian Journal of Physics* **1977**, *55* (5), 379-382.
58. Zeng, H.; Zhu, B.; Liu, K.; Fan, J.; Cui, X.; Zhang, Q. M., Low-frequency Raman modes and electronic excitations in atomically thin MoS₂ films. *Physical Review B* **2012**, *86* (24), 241301.
59. Ataca, C.; Şahin, H.; Ciraci, S., Stable, Single-Layer MX₂ Transition-Metal Oxides and Dichalcogenides in a Honeycomb-Like Structure. *The Journal of Physical Chemistry C* **2012**, *116* (16), 8983-8999.
60. Li, H.; Zhang, Q.; Yap, C. C. R.; Tay, B. K.; Edwin, T. H. T.; Olivier, A.; Baillargeat, D., From Bulk to Monolayer MoS₂: Evolution of Raman Scattering. *Advanced Functional Materials* **2012**, *22* (7), 1385-1390.
61. M Cardona; Guntherodt, G., Light Scattering in Solid II and III. *Topics in Applied Physics* **1982**, *50 & 51*.
62. Yu, P. Y.; Cardona, M., *Fundamentals of semiconductors : physics and materials properties*. 3rd, rev. and enlarged ed.; Springer: Berlin ; New York, 2001; p xviii, 639 p.
63. Bendow, B.; Birman, J. L., Theory of Resonant Raman Scattering in Crystals: A Generalized Bare-Exciton Approach. *Physical Review B* **1971**, *4* (2), 569-583.

Figures and Figure captions

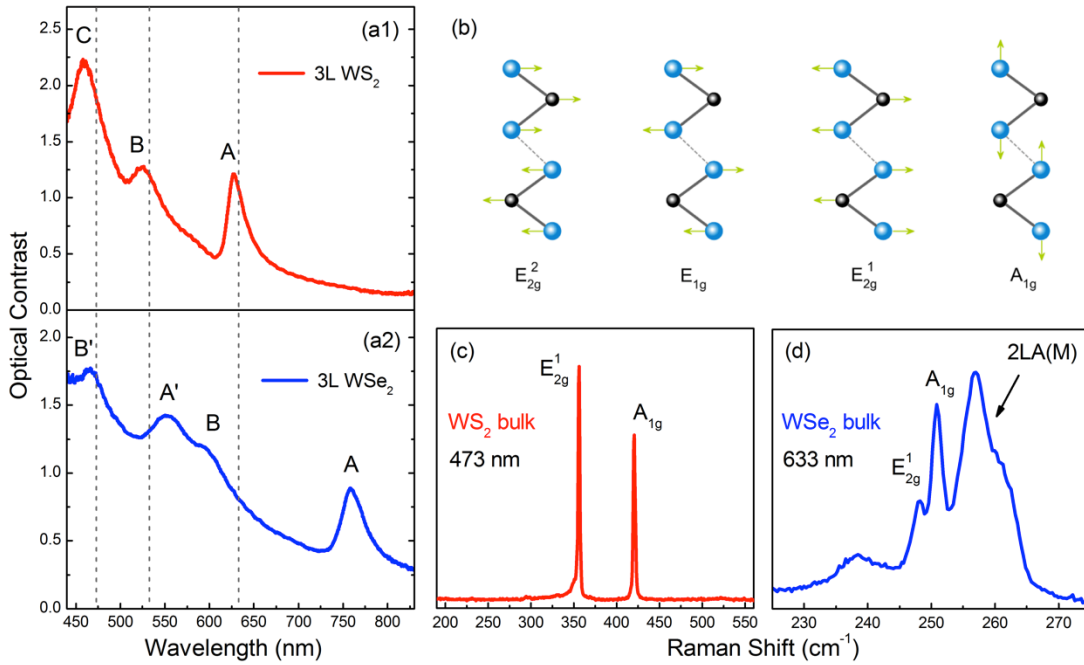


Figure 1 - Optical contrast of 3L (a1) WS₂ and (a2) WSe₂ flakes. The grey dashed arrows indicate wavelength of the excitation lasers used for Raman measurements. (b) Schematics showing atomic displacement of four Raman active modes in WS₂ and WSe₂. (c-d) Unpolarized Raman spectra of bulk (c) WS₂ and (d) WSe₂ obtained with 473 and 633 nm laser excitation, respectively.

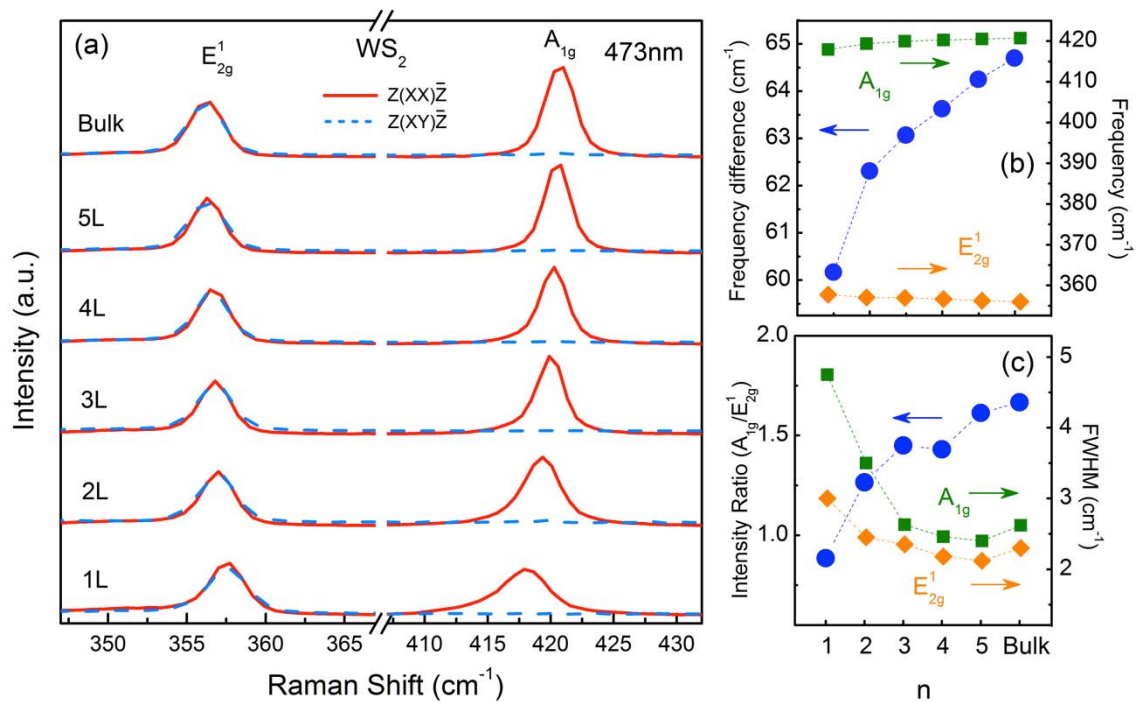


Figure 2 - (a) Raman spectra of 1 to 5L and bulk WS₂ flakes obtained in the parallel ($Z(XX)\bar{Z}$) and cross ($Z(XY)\bar{Z}$) polarization conditions obtained with 473 nm excitation. The spectra are normalized and vertically offset for clarity. (b) Position of the A_{1g} and E_{2g}^1 modes (right vertical axis) and their difference (left vertical axis) as a function of the number of layers (n). (c) Intensity ratio (left vertical axis) and FWHM (right vertical axis) of A_{1g} and E_{2g}^1 modes as a function of the number of layers. The spectral resolution is about 0.8cm^{-1} .

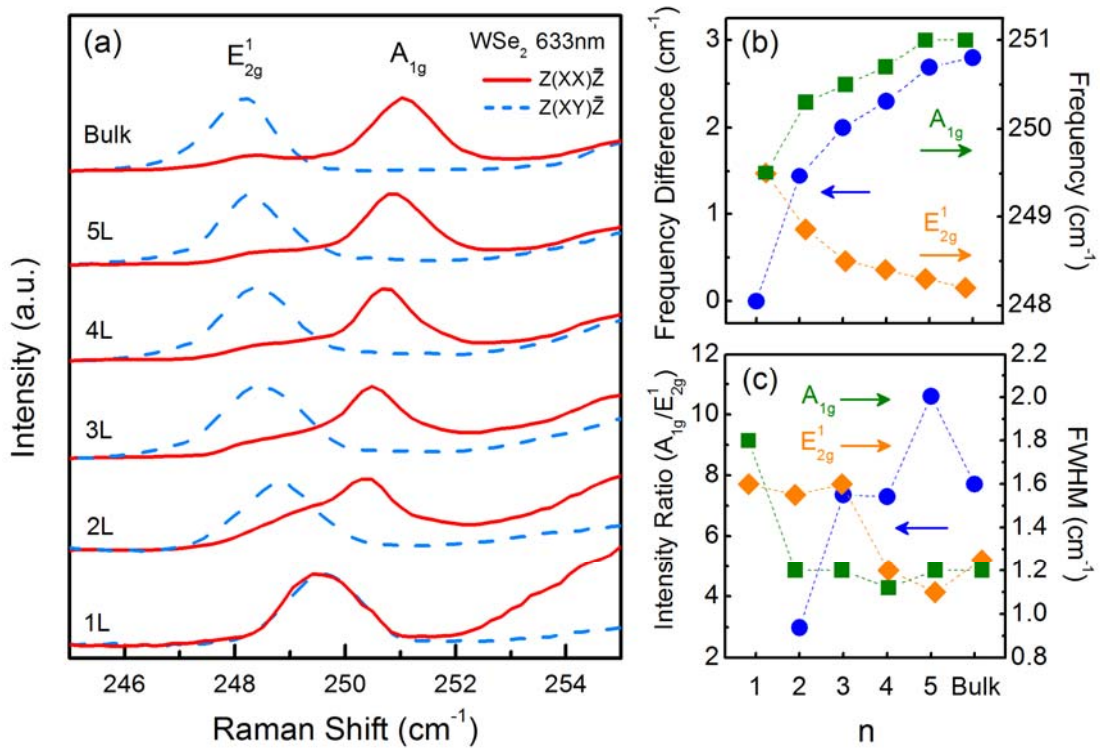


Figure 3 - (a) Raman spectra of 1 to 5L and bulk WSe₂ obtained in the parallel ($Z(XX)\bar{Z}$) and cross ($Z(XY)\bar{Z}$) polarization conditions obtained with 633 nm excitation. The spectra are normalized and vertically offset for clarity. (b) Position of the A_{1g} and E_{2g}^1 modes (right vertical axis) and their difference (left vertical axis) as a function of the number of layers (n). (c) Intensity ratio (left vertical axis) and FWHM (right vertical axis) of A_{1g} and E_{2g}^1 modes as a function of the number of layers. The spectral resolution is about 0.2cm^{-1} .

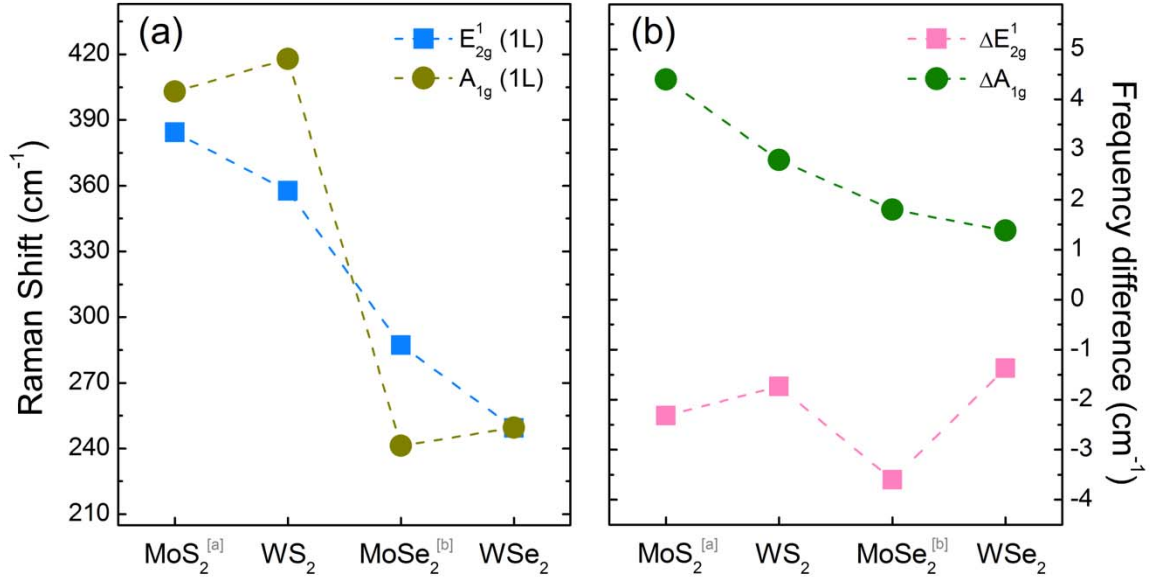


Figure 4 - (a) Frequency of the A_{1g} and E_{2g}^1 modes in monolayer MoS₂, WS₂, MoSe₂ and WSe₂ flakes. (b) Frequency difference (ΔA_{1g} and ΔE_{2g}^1) between monolayer and bulk flakes for A_{1g} and E_{2g}^1 modes for the four compounds. We define ΔA_{1g} and ΔE_{2g}^1 to be $\nu(A_{1g}(\text{bulk})) - \nu(A_{1g}(1\text{L}))$ and $\nu(E_{2g}^1(\text{bulk})) - \nu(E_{2g}^1(1\text{L}))$, respectively. The data for MoS₂ and MoSe₂ are obtained from Ref [42] and Ref [18], respectively.

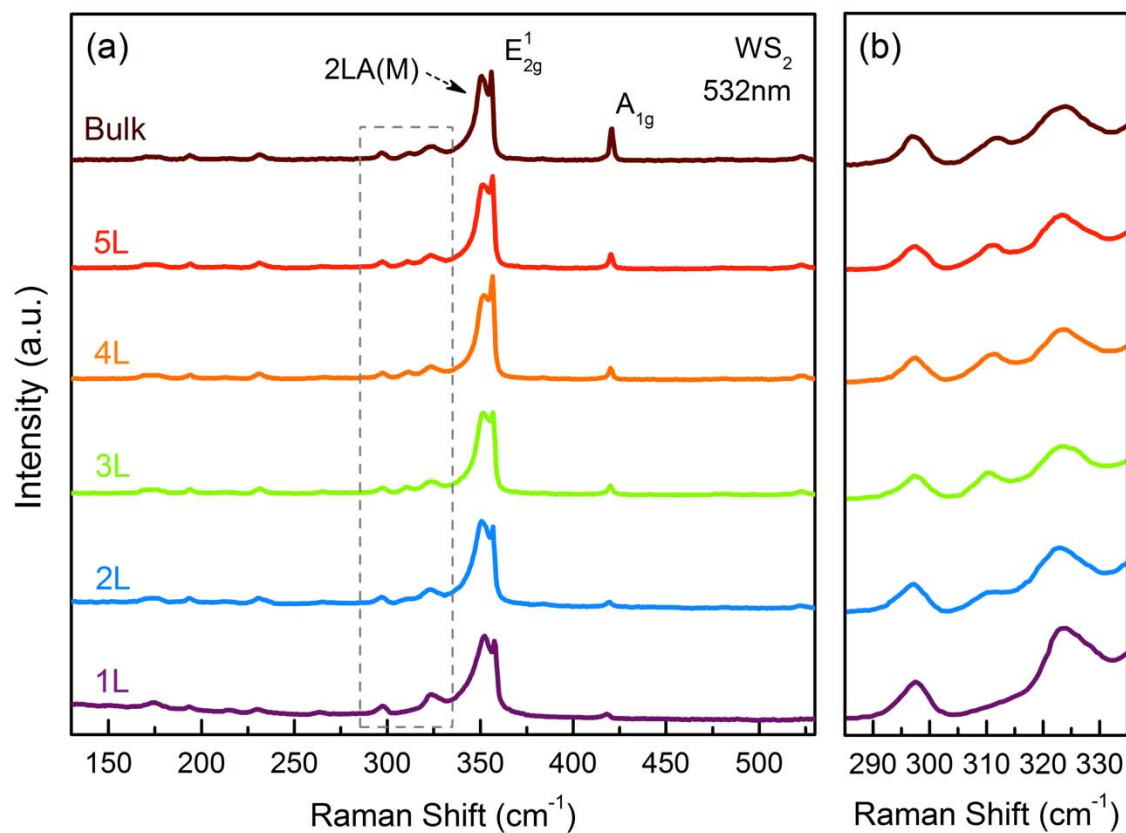


Figure 5 - (a) Unpolarized Raman spectra of 1 to 5L and bulk WS₂ flakes obtained with 532nm excitation. The spectra are normalized to the 2LA(M) peak and vertically offset for clarity. Part of the spectra indicated by a gray dashed rectangle in (a) is shown in larger scale in (b).

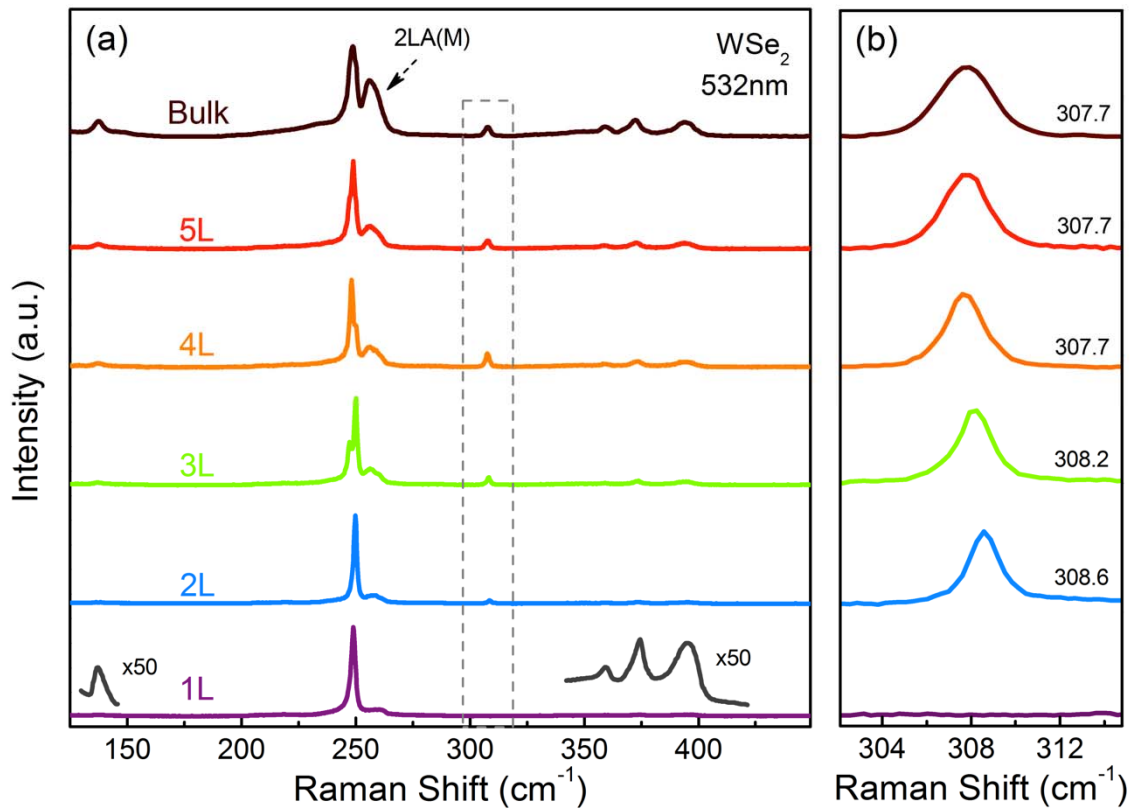
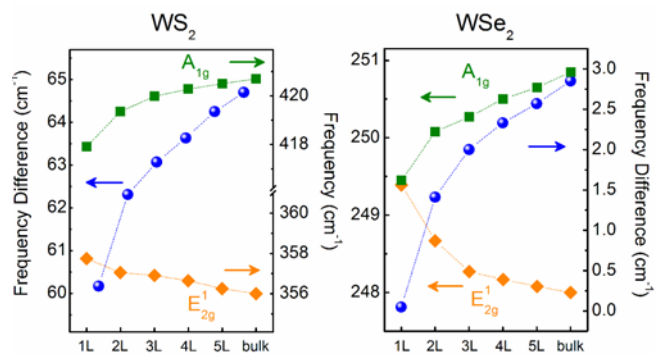


Figure 6 - (a) Unpolarized Raman spectra of 1 to 5L and bulk WSe_2 flakes obtained with 532 nm excitation. The spectra are normalized to the A_{1g} peak and vertically offset for clarity. Part of the spectra indicated by a gray dashed rectangle in (a) is shown in larger scale in (b). The numbers in (b) indicate the peak center positions.

Table of Contents Figure



Characteristic A_{1g} and E_{2g}^1 phonon modes for WS_2 and WSe_2 show distinct thickness dependence, which allows rapid identification of layer thickness.